Smart Structures and Systems, *Vol. 30, No. 2 (2022) 159-172*
https://doi.org/10.12989/sss.2022.30.2.159

Rod effects on transferred energy into SPT sampler using smart measurement system

Geunwoo Park [1a], Namsun Kim [1a], Won-Taek Hong [2b] and Jong-Sub Lee*[1]

[1] *School of Civil, Environmental and Architectural Engineering, Korea University, 145, Anam-ro, Seongbuk-gu, Seoul, 02841, Republic of Korea*
[2] *Department of Civil and Environmental Engineering, Gachon University, 1342, Seongnam-daero, Sujeong-gu , Seongnam-si, Gyeonggi-do, 13120, Republic of Korea*

(*Received September 2, 2021, Revised May 3, 2022, Accepted May 6, 2022*)

Abstract. To improve the accuracy of the standard penetration test (SPT) results, smart measurement system, which considers the energy transfer ratio into the sampler ($ETR_{Sampler}$), is required. The objective of this study is to evaluate the effects of joints and rod length on the transferred energy into the sampler. The energy transfer ratios into the rod head (ETR_{Head}) and $ETR_{Sampler}$, and the energy ratio from the head to the sampler (ER_{HS}) were obtained using energy modules, which were installed at the rod head and above the SPT sampler. Linear regression analyses are conducted to correlate the ER_{HS} with the number of joints, rod length, and SPT N-values. In addition, the dynamic resistances are calculated using both transferred energies into the rod head and into the sampler, and are compared with the corrected cone tip resistance measured from the cone penetration test (CPT). While the ETR_{Head} are generally constant, but the $ETR_{Sampler}$ and ER_{HS} gradually decrease along the depth or the number of joints, except at certain depths with high SPT N-values. Thus, the ER_{HS} can be estimated using the number of joints, rod length, and SPT N-values. The dynamic resistance evaluated by $E_{Sampler}$ produces a better correlation with the corrected cone tip resistance than that by E_{Head}. This study suggests that transferred energy into the SPT sampler may be effectively used for more accurate subsurface characterization.

Keywords: dynamic resistance; energy correction; energy module; standard penetration test (SPT); transferred energy

1. Introduction

Prior to the design and construction of an infrastructure, in situ tests are conducted to characterize the subsurface and determine the engineering properties of the soils. The standard penetration test (SPT) is one of the most popular in situ tests, and the driving rod is penetrated by dropping a hammer at a constant potential energy (473.5 N·m) during the SPT. The number of blows required for a 30 cm deep penetration are recorded as the SPT N-value after 15 cm of initial penetration (Decourt *et al*. 1988, Clayton 1995). The SPT N-value represents the strength characteristics of the ground at each depth, and soil properties such as cohesion, internal friction angle, and relative density were estimated using several SPT N-value empirical equations (Melzer 1971, Marcuson and Bieganousky 1977, Skempton 1986, Kulhawy and Mayne 1990, Hatanaka and Uchida 1996, Cubrinovski and Ishihara 1999, Das *et al*. 2012). The SPT is most widely used due to its simplicity, convenience, and applicability compared to the other in situ tests. In addition, the SPT has been studied and applied in several cases such as geotechnical investigation, liquefaction, and pile foundation, etc. (Bahari *et al*. 2020, Seo *et al*. 2021), thus, the SPT N-value is used with many empirical correlations.

Despite the advantages of the SPT, the test results obtained may be less accurate depending on the experimental conditions, resulting from an inconsistent driving energy (Sjoblom *et al*. 2002). Therefore, the transferred energy at the SPT rod head was measured using the energy module, and the SPT N-values were corrected using the measured transferred energy (Schmertmann and Palacios 1979, Kovacs and Salomone 1982, Butler *et al*. 1998, Sjoblom *et al*. 2002). The measured transferred energy is lower than the potential energy of the drop hammer due to the energy loss at the anvil and inconsistent driving energy. Note that the SPT N-values, which are corrected using the transferred energy at the rod head with a reference energy ratio of 60%, have been used to estimate engineering parameters (Hettiarachchi and Brown 2009, Mujtaba *et al*. 2018, Ghali *et al*. 2020).

The actual penetration energy of the split spoon sampler may be lower than the transferred energy at the rod head because of the energy loss in the extended driving rods. The energy loss contributes to the inaccuracy of the estimation of the engineering parameters based on the corrected SPT N-value using the transferred energy at the head of the driving rods. Several studies have been conducted on the measurement of the energy near the cone tip to compensate for the inaccuracy of the energy correction at the head of the driving rods. Kianirad *et al*. (2011) also installed an

*Corresponding author, Ph.D., Professor,
E-mail: jongsub@korea.ac.kr
[a] Ph.D. Student
[b] Ph.D., Professor

ISSN: 1738-1584 (Print), 1738-1991 (Online)

accelerometer and a load cell at the cone tip of a dynamic cone penetrometer and analyzed the force signal with account of the energy loss. In addition, Byun *et al*. (2014) and Kim *et al*. (2019) measured the energies at the rod head and tip using a dynamic cone penetrometer, and the strength of the ground was evaluated based on these energies. Furthermore, Lee and Byun (2020) developed an instrumented cone penetrometer and studied its dynamic and static resistances under the same ground conditions. These studies were conducted using portable dynamic penetrometer.

Lukiantchuki *et al*. (2011) installed an accelerometer and a load cell outside just above the SPT sampler and measured the dynamic responses to evaluate the transferred energies. Note that these sensors had durability issues because they were installed externally. Hong *et al*. (2022) instrumented energy modules incorporated with an accelerometer and a load cell inside. The energy modules were located at the rod head and above the SPT sampler to measure the transferred energies. They showed that the transferred energy into the SPT sampler was less than that into the rod head. Note that the mechanism of the energy loss in the SPT sampler has not studied in details.

The objective of this study is to evaluate the effects of rod and ground parameters on the energy transfer ratio from the head to the sampler in the SPT. SPT tests were performed on weathered soils at three sites to measure the transferred energies at the rod head and above the SPT sampler. The energy ratio was calculated using the measured transferred energies at the rod head and above the SPT sampler. The calculated energy ratio was subsequently correlated with the number of joints, the rod length and the SPT N-value using multiple regression analysis. In addition, the calculated dynamic resistances were compared with the measured static resistances. This study presents the effects of the rods on the energy loss using smart measurement system of the transferred energy at the SPT sampler. The paper first explains the background theories including N-value correction, transferred energy at the SPT head, energy losses, and dynamic resistance. Second, the specifications of the energy module are provided, and this paper describes the field study. Finally, the test results obtained at the three sites are analyzed and discussed.

2. Background theory

2.1 N-value correction by measuring transferred energy

In an SPT, the transferred energy (E), which is calculated using the force-velocity (F-V) method (ASTM D4633), can be obtained from the following integration equation

$$E(t) = \int F_S(t) \times V_a(t) dt \tag{1}$$

where F_s is the force measured by the load cell, and V_a is the velocity calculated by integrating the measured acceleration and is equivalent to the particle velocity. The force obtained from the accelerometer (F_a) can be calculated by multiplying V_a with the impedance (Z) as follows

$$F_a(t) = Z \times V_a(t) \tag{2}$$

where Z can be represented as a function of the elastic modulus (E_s), cross-sectional area (A), and longitudinal wave velocity (C) of the rod as follows

$$Z = \frac{E_s A}{C} \tag{3}$$

Thus, Eq. (2) is replaced as follows

$$F_a(t) = \frac{E_s A}{C} \times V_a(t) \tag{4}$$

The energy transfer ratio (ETR), which is defined as the percent ratio of the calculated E to the theoretical potential energy (PE), is used to correct the SPT N-value. In general, the corrected SPT N-value for a reference energy ratio of 60% (N_{60}) is calculated based on an ETR (Seed *et al*. 1985) as follows

$$N_{60} = \frac{ETR}{60} \times N \tag{5}$$

In general, the ETR is calculated using the transferred energy into the rod head (E_{Head}). However, the transferred energy into the SPT sampler ($E_{Sampler}$) exhibits a greater influence on the dynamic penetration resistance than E_{Head}. Therefore, the ETR calculated using the $E_{Sampler}$ is more reasonable for an accurate correction of the dynamic penetration resistance than that calculated using the E_{Head} (Byun and Lee 2013, Byun *et al*. 2014). On the other hand, the normalized SPT N-value, $(N_1)_{60}$, considers the effects of the ETR, rod length, liner, borehole diameter, overburden, and blow count frequency as follows

$$(N_1)_{60} = \frac{ETR}{60} \cdot C_R \cdot C_S \cdot C_B \cdot C_N \cdot N \tag{6}$$

where C_R is the rod length correction factor, C_S is the liner correction factor, C_B is the borehole diameter correction factor, and C_N is the overburden correction. The rod length correction factor (C_R) suggested by Skempton (1986), Bowles (1996), and Robertson and Wride (1997) is summarized in Table 1. Table 1 shows that $(N_1)_{60}$ is not affected for a rod length over 10 m (C_R = 1) but is underestimated for a rod length under 10 m (C_R < 1) (Skempton 1986, Bowles 1996).

Table 1 Rod length correction factor

Length of driving rod [m]	Rod length correction factor [-]
0 ~ 4	0.75
4 ~ 6	0.85
6 ~ 10	0.95
10 ~	1

2.2 Transferred energy into the SPT rod head according to rod length

In previous studies, the transferred energy into the rod head was measured according to the length of the driving rod by using an energy module during SPT (Kovacs 1979, Kovacs and Salomone 1982, Butler *et al*. 1998). Test results showed that the amplitude of the compression wave was peak below the anvil, in which the sensors were installed, and then was gradually decreased according to travel time. Furthermore, until the tensile wave arrived after hammer impact, more than 90% of the total energy was transferred (Lee *et al*. 2001, 2010). Note that the arrival time of the initial tensile wave is equal to the round-trip time (t = 2L/C), where L is the length of the driving rods and C is the speed of the longitudinal wave. Therefore, the arrival time of the initial tensile wave is proportional to the length of the driving rods (Schmertmann and Palacios 1979).

As the length of the rod increases, the travel time of the initial tensile wave is delayed, and the area of the initial compression wave subsequently increases. Consequently, the calculated transferred energy increases with an increase in the length of the rod. Force signals measured by the load cell are plotted in Fig. 1 according to the length of the driving rods. Fig. 1 shows that as the rod length increases, the first arrival time of the initial tensile wave (open circles in Fig. 1) proportionally increases. The increment in the initial compressive area, however, gradually decreases with an increase in the rod length. Thus, Skempton (1986) and Bowles (1996) reported that the SPT N-value was unaffected by the rod length, if the rod length is greater than 10 m, because the energy was sufficiently transferred from the rod head to the SPT sampler. The rod length correction factor (C_R) was used for short rod lengths, in which the tensile wave reflected earlier (Skempton 1986). Energy losses according to the numbers of joints, however, were not considered in the rod length correction factor (C_R).

2.3 Energy losses in transferred energy

For the measurement of the transferred energy into the rod head, the energy module has been commonly installed between the rod head and the anvil. Thus, the measured transferred energy considered energy loss occurred at the hammer and anvil. For the SPTs in deep layers, rods should be extended. Thus, energy losses may occur not only at the anvil but also at the joints of the driving rods due to transmissions and reflections of elastic waves caused by the impedance mismatch at the joints as shown in Fig. 2. Incident waves, which are generated by a dynamic blow, are mostly transmitted, and the remaining incident waves are reflected at each joint. These transmissions and reflections yield the energy losses (Byun and Lee 2013). Thus, the transferred energy into the SPT sampler is smaller than that into the rod head.

2.4 Dynamic resistance

In the SPT, the penetration energy ($E_{Penetraion}$), which is the energy used to penetrate the sampler into the ground, can be estimated using from the potential energy, neglecting the energy loss caused by the hammer, rod, and so on (Odebrecht *et al*. 2004). Therefore, $E_{Penetration}$ is defined as the work done (W_s) on the sampler soil system (Schnaid *et al*. 2009). W_s is expressed as the product of the dynamic reaction force (F_d) and penetrated depth or displacement (d). Thus, $E_{Penetration}$ is

$$E_{Penetration} = W_s = F_d \cdot d \tag{7}$$

The dynamic reaction force (F_d) is represented by the product of the dynamic resistance (q_d) and cross-sectional area of the cone (A_c) as follows

$$F_d = q_d \cdot A_c \tag{8}$$

Substituting Eq. (8) into Eq. (7), the dynamic resistance (q_d) is expressed as follows

$$q_d = \frac{E_{Penetration}}{A_c \cdot d} \tag{9}$$

For the dynamic penetration test using the energy module, q_d can be calculated using the measured acceleration and force (Byun *et al*. 2014, Kim *et al*. 2019, Lee *et al*. 2019). The displacement (d) can be calculated by integrating the velocity (V_a), which is obtained by integrating the measured acceleration. According to the law of energy conservation, the transferred energy at the rod as

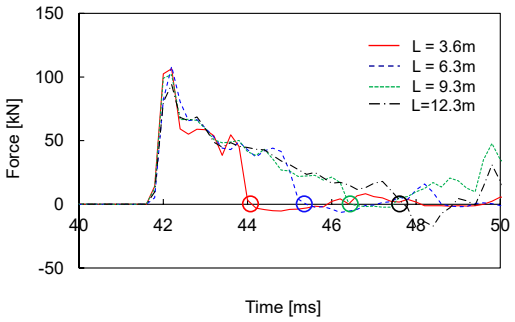

Fig. 1 Force signals (F_s) measured at the head of the driving rod according to the length of driving rods. Open circles (○) denote the first arrival time of tensile wave

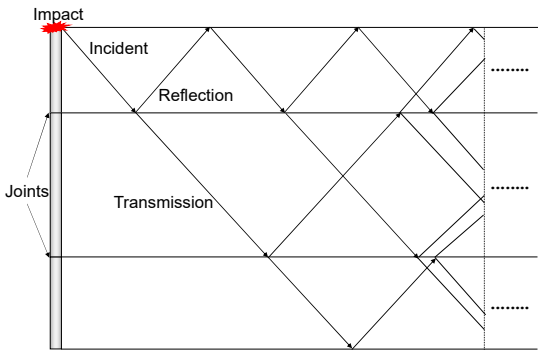

Fig. 2 Schematic drawing of attenuation concepts. The thickness of arrows denotes the intensity of energy

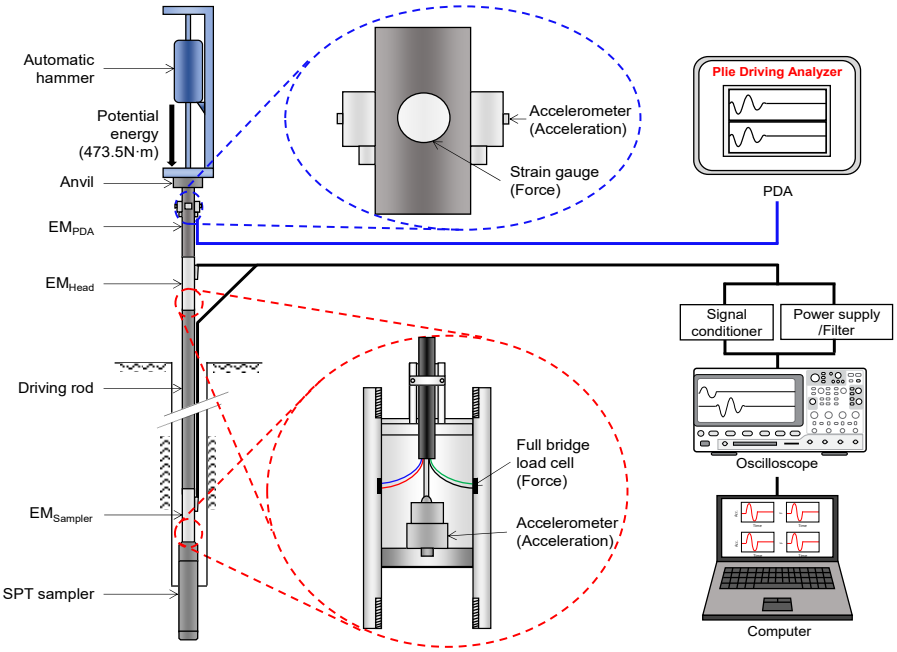

Fig. 3 Schematic drawing of standard penetration test and energy modules. EM denotes the energy module

described in Eq. (1) is equal to the penetration energy as described in Eq. (8). The dynamic resistance (q_d) is expressed as follows

$$q_d = \frac{\int F_s(t) \times V_a(t)dt}{A_c \cdot \int V_a(t)dt} \quad (10)$$

The dynamic resistance (q_d) is calculated using the measured forces and accelerations from the energy module. The dynamic resistance (q_d) calculated by Eq. (10) may be directly compared with the corrected cone tip resistance (q_t) obtained from the cone penetration test (CPT) if rheological properties of soils are negligible. The penetration rate of the SPT is 100-200 times faster than that of the CPT. Note that the damping effect is negligible for both dynamic resistance (q_d) and cone tip resistance (q_t) in coarse-grained soils. In addition, as q_d and q_t are not affected by the particle size or density in non-plastic ground, both penetration resistances are comparable in sandy and silty soils (Schnaid *et al.* 2017).

3. Energy module and system

3.1 Energy losses in transferred energy

In this study, the transferred energies into the rod head and into the SPT sampler were measured using the energy modules installed at the rod head (EM_{Head}) and above the SPT sampler ($EM_{Sampler}$) as shown in Fig. 3. The outer diameters of the EM_{Head} and $EM_{Sampler}$ are equal to that of the SPT driving rod. The accelerometer and load cell configured with full-bridge strain gauges are installed at the inner region of EM_{Head} and $EM_{Sampler}$ for protection of the sensors as shown in Fig. 3 (Yoon and Lee 2012, Byun *et al.* 2015, Hong *et al.* 2016, 2022). The shock type accelerometer (model 350C03, PCB) could measure up to 10,000 g along the uni-axis. The load cell was fabricated with strain gauges with an electrical resistance of 120 Ω. The accelerometer was installed at the center of the rod and full-bridged four strain gauges were attached on the opposite side of the rod as shown in Fig. 3 to compensate the temperature and eccentricity (Byun *et al.* 2013). In addition, the commercial SPT energy module (EM_{PDA}), which is manufactured by PDI, was used to measure the transferred energy into the rod head by connecting to the pile driving analyzer (PDA). In this system, the accelerometers and strain gauges based load cell were installed outside EM_{PDA}.

3.2 Measurement system

The different measurement systems were used for types of energy modules. In the measurement system of EM_{PDA}, signals from accelerometers and strain gauges were gathered, filtered, and analyzed by the pile driving analyzer (PDA). The measurement system of EM_{Head} and $EM_{Sampler}$ consists of power supply, filter, signal conditioner, and oscilloscope. Input voltage and low pass filtering frequency were set to 1 V and 20 kHz, respectively. The oscilloscope measured the signals at the sampling rate of 96 kHz. The obtained data were monitored and saved using a laptop computer.

4. Field study

4.1 Site description

In this study, SPTs were conducted until a depth of 14.3 m at three sites in Korean (Hanam, Gongju, and Pohang), which are labeled as BH-H (Hanam), BH-G (Gongju), and BH-P (Pohang) for convenience. The soil profiles of the three sites based on the SPTs are shown in Fig. 4. For the

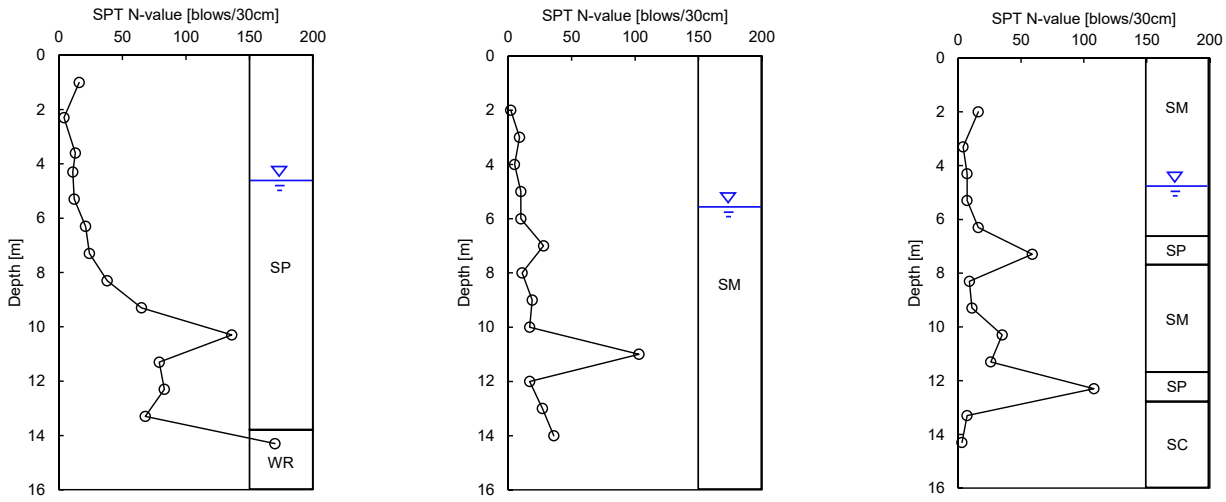

(a) At BH-H (b) At BH-G (c) At BH-P

Fig. 4 Profiles of SPT N-value according to depth (SP, WR, SM and SC denote the poorly graded sand, weathered rock, silty sand, and clayey sand, respectively)

BH-H site, the SPTs were conducted at depth of 1 m, 2.3 m, 3.8 m, 4.3 m and at 1 m intervals from the depth of 4.3 m as shown in Fig. 4(a). Low SPT N-values were obtained at shallow depths, and these values gradually increase after 7.3 m. At 14.3 m, in which the ground is weathered rock, the SPT N-value is greater than 170 blows/30 cm, and thus, the SPT was completed at this site. The SPT N-values obtained at BH-G and BH-P are plotted in Figs. 4(b) and 4(c), respectively. For the BH-G site, at a depth of 11.3 m, the SPT N-value is approximately 100 blows/30 cm; however, the average SPT N-values at other depths is approximately 40 blows/30 cm. Note that SPT N-values gradually increase along the depth except at the depth of 11.3 m. For the BH-P site, the SPT N-value is 100 blows/30 cm at the depth of 12.3 m, and extremely low SPT N-values (3-7 blows/30 cm) were obtained after this depth, in which the ground is composed of clayey sand.

For the BH-P site, the CPT was conducted at a distance of 5 m from the SPT borehole. The CPT was conducted after a 2.5 m excavation, and the cone tip resistance and pore pressure were subsequently measured according to the depth up to depth of 14.3 m. In addition, the measured cone tip resistances were corrected using the pore pressure. Moreover, the corrected cone tip resistances were compared with the SPT results.

Disturbed specimens were obtained from the SPT at each depth, and index property tests were conducted. First, sieve analyses conducted based on ASTM D422 produced D_{10}, D_{30}, D_{50}, D_{60}, the coefficient of uniformity (C_u), and curvature (C_g). In addition, the specific gravity, and the maximum and minimum void ratios were determined based on ASTM D854, ASTM D4253, and ASTM D4254, respectively. Finally, the liquid and plastic limits, and the plastic index were obtained according to ASTM D4318. The calculated index properties are listed in Table 2.

Table 2 Index properties at BH-H, BH-G, and BH-P

Site	Depth [m]	C_u	C_g	G_s	LL [%]	PL [%]	PI [%]	Remarks
H	~ 4.3	5.8	3.1	2.70	43.9	21.5	22.4	SP
	5.3 ~ 6.3	7.0	4.5	2.71	39.5	18.2	21.3	
	7.3 ~ 8.3	8.5	2.5	2.67	41.3	16.5	24.8	
	9.3 ~ 10.3	4.5	1.6	2.68	40.5	22.5	18	
	11.3 ~ 12.3	10.3	5.8	2.65	35.8	19.5	16.3	
	13.3 ~ 14.3	12.5	7.5	2.61	32.5	18.7	13.8	WR
G	~ 4.3	6.2	2.5	2.71	44.5	19.5	25	SM
	5.3 ~ 6.3	4.2	3.3	2.69	48.6	21.2	27.4	
	7.3 ~ 8.3	3.5	2.1	2.68	47.5	22.5	25	
	9.3 ~ 10.3	6.3	2.1	2.70	43.6	18.5	25.1	
	11.3 ~ 12.3	5.2	3.3	2.69	45.2	19.9	25.3	
	13.3 ~ 14.3	4.4	2.3	2.68	44.0	18.5	25.5	
P	~ 4.3	5.8	2.3	2.69	44.2	21.5	22.7	SM
	5.3 ~ 6.3	4.2	2.3	2.70	45.5	22.2	23.3	
	7.3 ~ 8.3	3.2	1.5	2.71	46.5	23.2	23.3	SP
	9.3 ~ 10.3	4.5	2.5	2.71	49.3	25.4	23.9	SM
	11.3 ~ 12.3	2.5	3.2	2.74	48.5	22.5	26	SM-SP
	13.3 ~ 14.3	1.5	1.2	2.78	44.2	21.5	22.7	SC

*SP, WR, SM and SC denote the poorly graded sand, weathered rock, silty sand, and clayey sand, respectively

4.2 Calculation of transferred energy

Two energy modules (EM_{Head} and $EM_{Sampler}$) were used at the BH-G and BH-P. Note that three energy modules (EM_{PDA}, EM_{Head}, and $EM_{Sampler}$) were used at the BH-H site. Force time waveforms were obtained from the signals, which were measured at these modules, and the energy time waveforms were calculated using the F-V method. The waveforms obtained at a depth of 3.3 m at BH-H are plotted in Fig. 5. Figs. 5(a), 5(b), and 5(c) show the force time waveforms measured at EM_{PDA}, EM_{Head}, and $EM_{Sampler}$,

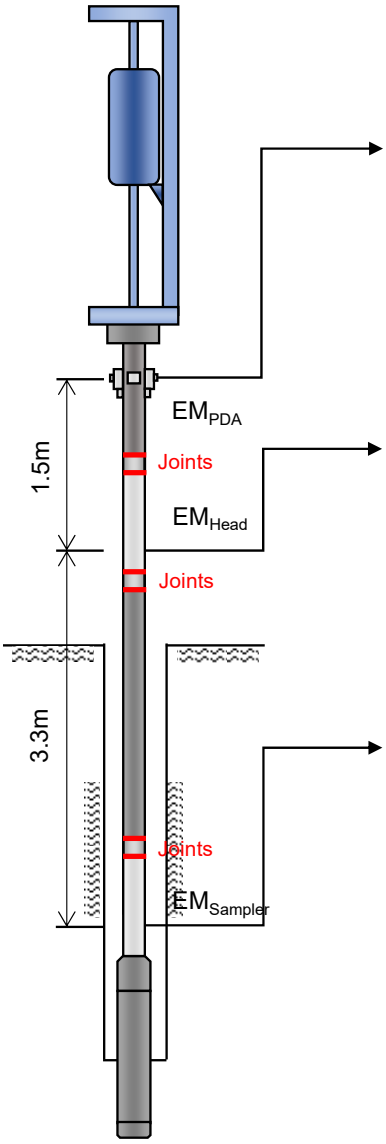

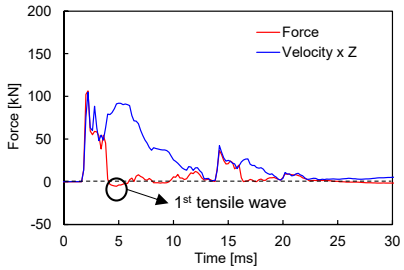

(a) Force time waveform at rod head measured by EMPDA

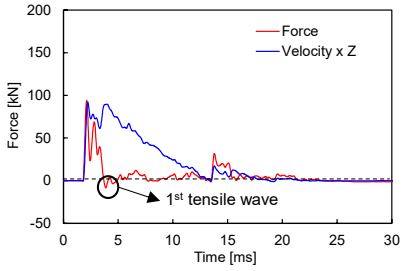

(b) Force time waveform at rod head measured by EMHead

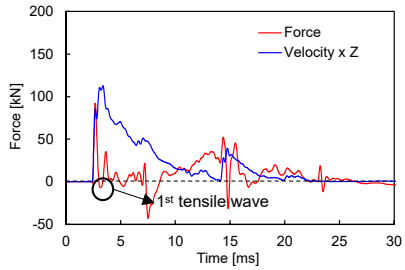

(c) Force time waveform at SPT sampler measured by EMSampler

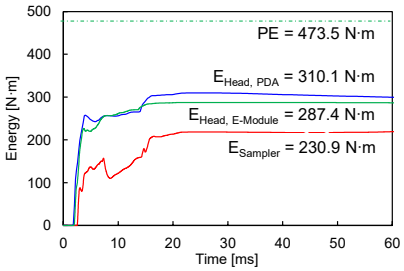

(d) Energy time waveform

Fig. 5 Measured dynamic responses

respectively. Both the force time waveforms measured by the EM_{PDA} and EM_{Head} as shown in Figs. 5(a) and 5(b) show a similar tendency. Note that the first tensile wave was generated earlier in the force time waveform of the $EM_{Sampler}$ (Fig. 5(c)) than in the other force time waveforms (Figs. 5(a) and 5(b)).

The transferred energies calculated using the force time waveforms measured by three energy modules are plotted in Fig. 5(d). Fig. 5(d) shows that the measured transferred energies at EM_{PDA}, EM_{Head}, and $EM_{Sampler}$ are 310.1, 287.4, and 230.9 N·m, respectively. The measured transferred energy gradually decreases with the distance from the top. In addition, EM_{PDA} and EM_{Head} are 1.5 m apart with two joints between them. The difference between the measured transferred energies at EM_{PDA} and EM_{Head} is 22.7 N·m. EM_{Head} and $EM_{Sampler}$ are 3.3 m apart with four joints between them. The difference between the measured transferred energies at EM_{Head} and $EM_{Sampler}$ is 56.5 N·m. The difference between the measured transferred energies at each energy module increases with an increase in the distance or in the number of joints between energy modules.

4.3 Transferred energy ratio into the rod head and the sampler

The force and velocity waveforms were obtained using the EM_{PDA} and $EM_{Sampler}$ in three sites. The energy transfer ratios into the rod head (ETR_{Head}) and into the sampler ($ETR_{Sampler}$) calculated using the waveforms obtained from EMPDA and $EM_{Sampler}$ based on the F-V method are plotted in Fig. 6. Fig. 6(a) shows that the range of ETR_{Head} is 60%–75%, and it tends to either remain constant or increases

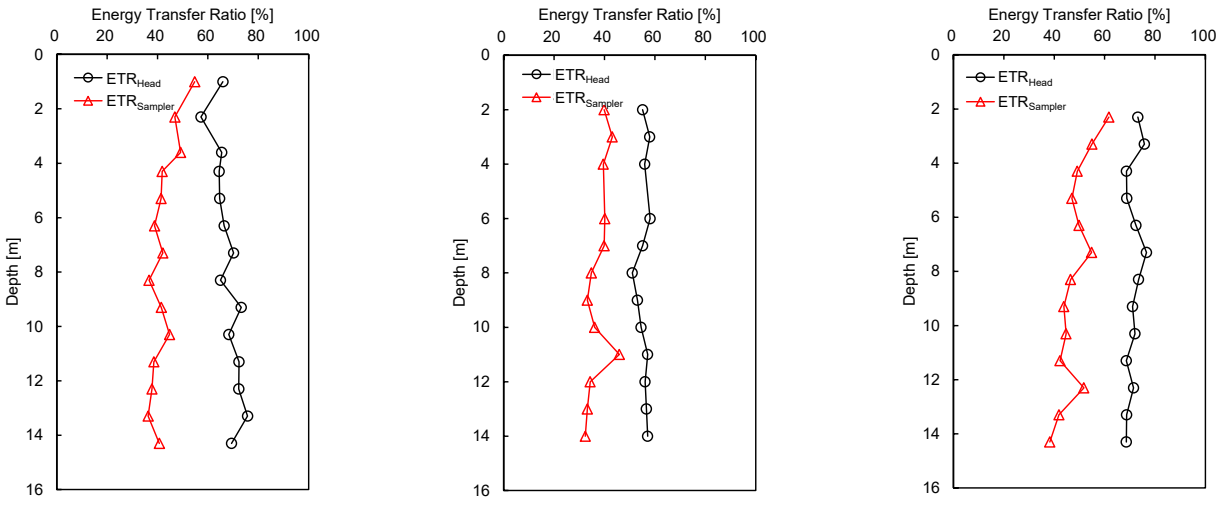

(a) At BH-H (b) At BH-G (c) At BH-P

Fig. 6 Calculated energy transfer ratio into rod head and sampler according to depth

slightly as the depth increases at the BH-H site. In addition, the average $ETR_{Sampler}$ is approximately 45%, and it tends to gradually decrease according to the depth increases, contrary to ETR_{Head}. The difference between ETR_{Head} and $ETR_{Sampler}$ increases from 11% to 29% as the depth increases.

Fig. 6(b) shows the ETR_{Head} and $ETR_{Sampler}$ of the BH-G site according to the depth. The average ETR_{Head} and $ETR_{Sampler}$ are 55% and 40%, respectively. ETR_{Head} is almost constant along the depth. $ETR_{Sampler}$ slightly decreases according to the depth, except at a depth of 11 m. Soil profile of the BH-G site shows that SPT N-values at a depth of 11.3 m are highest as shown in Fig. 4(b). The highest SPT N-value may produce the highest $ETR_{Sampler}$ at the depth of 11.3 m. Fig. 6(c) shows that at the BH-P site the ETR_{Head} is almost 70% at entire depth, and the $ETR_{Sampler}$ decreases from 62% to 38% according to the depth. The higher SPT N-values at depths of 7.3 m and 11.3 m as shown in Fig. 4(c) produce the higher $ETR_{Sampler}$ values.

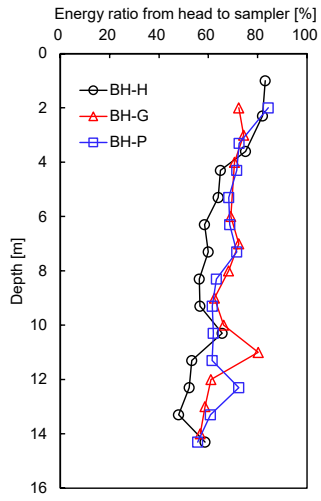

Fig. 7 Energy transfer ratio from head to sampler (ERHS) according to depth

To evaluate the effect of the joints and rod length on the energy loss, the energy ratio from the head to the sampler (ER_{HS}), which is the ratio of the transferred energy into the SPT sampler to that into the head, is estimated as follows

$$ER_{HS}(\%) = \frac{E_{Sampler}}{E_{Head}} \times 100 \tag{11}$$

The calculated ER_{HS} at three sites according to the depth is plotted in Fig. 7. The ER_{HS} at the BH-H site shows a tendency to gradually decrease with depth. Its values at depths of 10.3 m and 14.3 m are higher than those at other depths. The ER_{HS} at the BH-G site tends to decrease as the depth increases, similar to that obtained at the BH-H site; in contrast, the ER_{HS} at a depth of 11 m with a higher SPT N-value is higher than that at other depths. The ER_{HS} at the BH-P site tends to gradually decrease with depth, similar to that obtained at the other two sites; however, the higher values of ER_{HS} were measured at depths of 7 m and 12 m with higher SPT N-values. As a result, the higher ER_{HS} were obtained at depths with higher SPT N-values, and the ER_{HS} decreases as the depth increases for other depths.

4.4 Corrected N-values

The corrected SPT N-values (N_{60}) described in Eq. (4) have been commonly obtained by using the transferred energy into the rod head. In this study, the N_{60} was calculated using ETR_{Head} (N_{60_Head}) and $ETR_{Sampler}$ ($N_{60\_Sampler}$). The calculated N_{60_Head} and $N_{60\_Sampler}$ according to the depth are represented in Fig. 8. Fig. 8(a) shows that $N_{60\_Sampler}$ is smaller than N_{60_Head}, and the difference between both N_{60} gradually increases as the depth increases for the BH-H site. Figs. 8(b) and 8(c) show that $N_{60\_Sampler}$ is generally smaller than N_{60_Head} for the BH-G and BH-P sites. For the BH-G site, the difference between N_{60_Head} and $N_{60\_Sampler}$ generally increases with depth, except at a depth of 11.3 m. In addition, the minor difference between N_{60_Head} and $N_{60\_Sampler}$ at the depths of 13.3 m and 14.3 m for the BH-P site may result from the

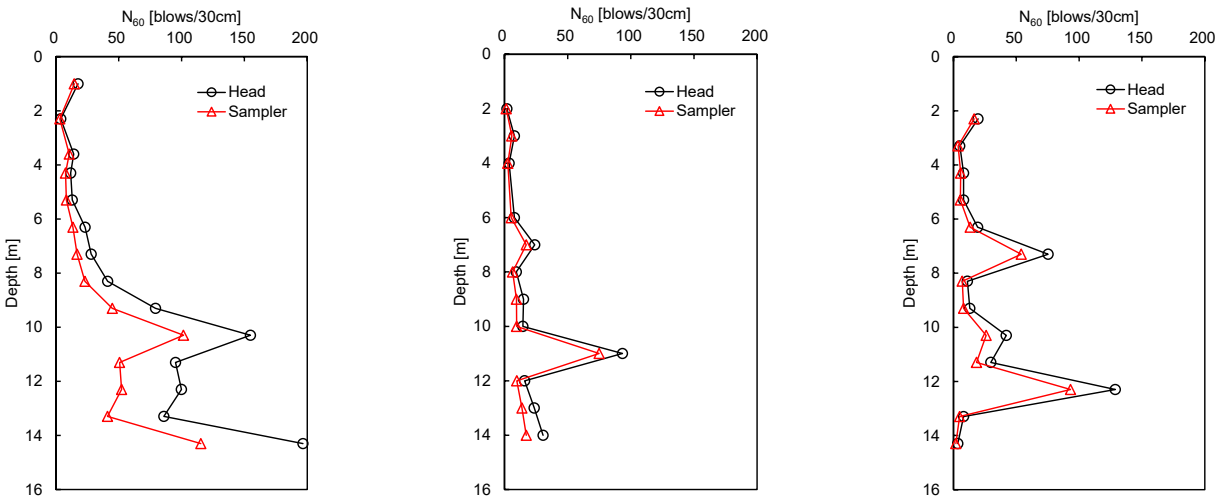

(a) At BH-H (b) At BH-G (c) At BH-P

Fig. 8 Corrected N-value (N60) by the reference energy efficiency of 60% based on transferred energies into rod head and sampler

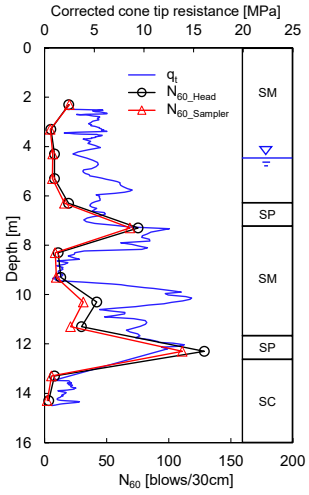

Fig. 9 Corrected cone tip resistance (q_t) and energy corrected SPT N-value (N_{60}) using energies transferred into rod head and sampler (SP, WR, SM and SC denote the poorly graded sand, weathered rock, silty sand, and clayey sand, respectively)

clayey sandy soils.

4.5 Comparison with CPT results

At the BH-P site, the CPT was conducted at a distance of 5 m from the SPT borehole. According to the depth, from the cone tip resistance and pore pressure the corrected cone tip resistance (q_t) was obtained. The calculated q_t was compared with the calculated N_{60_Head} and $N_{60\_Sampler}$, as shown in Fig. 9. The soil type is silty sand up to 6.3 m depth, the maximum calculated N_{60} is 20 blows/30 cm, and q_t is approximately 5 MPa. At a depth of 7.3 m, N_{60_Head} and $N_{60\_Sampler}$ are 75 blows/30 cm and 54 blows/30 cm, respectively, and q_t is approximately 13 MPa. At depths of 8.3 m and 9.3 m, q_t is 2.5 MPa, in which N_{60} is under 20 blows/30 cm. The corrected cone tip resistance (q_t) is 14–15 MPa at depths of 10.3 m and 12.3 m, in which $N_{60\_Sampler}$ and N_{60_Head} are greater than 40 blows/30 cm, and greater than 100 blows/30 cm, respectively. Fig. 9 shows that N_{60_Head}, $N_{60\_Sampler}$, and q_t tend to be proportional to each other.

5. Analyses and discussion

5.1 Effects of soil properties

The energy transfer ratio into the sampler ($ETR_{Sampler}$) at the three sites generally decreases with the depth as shown in Fig. 6. However, the higher $ETR_{Sampler}$ were obtained with the higher SPT N-values, therefore, the SPT N-values may influence the energy transfer ratio. For the evaluation of the ground condition effect on the $ETR_{Sampler}$, ER_{HS}, the SPT N-values, and the ground condition at each site according to the depth are represented in Fig. 10. Fig. 10(a) shows that up to the depth of 7.3 m, in which the SPT N-value is less than 30 blows/30 cm, the SPT N-value slightly increases, but ER_{HS} gradually decreases with an increase in the depth. However, the ER_{HS} at depths of 11.3 m and 14.3 m, in which SPT N-values are higher than 100 blows/30 cm, are approximately 10% higher than those at near depths for the BH-H site. In addition, the ER_{HS} at 11 m depth of the BH-G site, and 12.6 m depth of BH-P site, in which the SPT N-value is more than 100 blows/30 cm, are higher than that at other depths. However, the ER_{HS} at other depths, in which the SPT N-value is less than 30 blows/30 cm, decreases according to the depth regardless of the SPT N-value.

For the estimation of the effect of the SPT N-value on ER_{HS}, the force and energy time waveforms measured by EM_{PDA} and $EM_{Sampler}$ at depths of 12.3 m (N = 108 blows/30 cm) and 14.3 m (N = 3 blows/30 cm) at the BH-P site are represented in Fig. 11. Force time waveforms measured by EM_{PDA} plotted in Fig. 11(a) show the initial compression waves up to the time of 2L/C after impact. Furthermore,

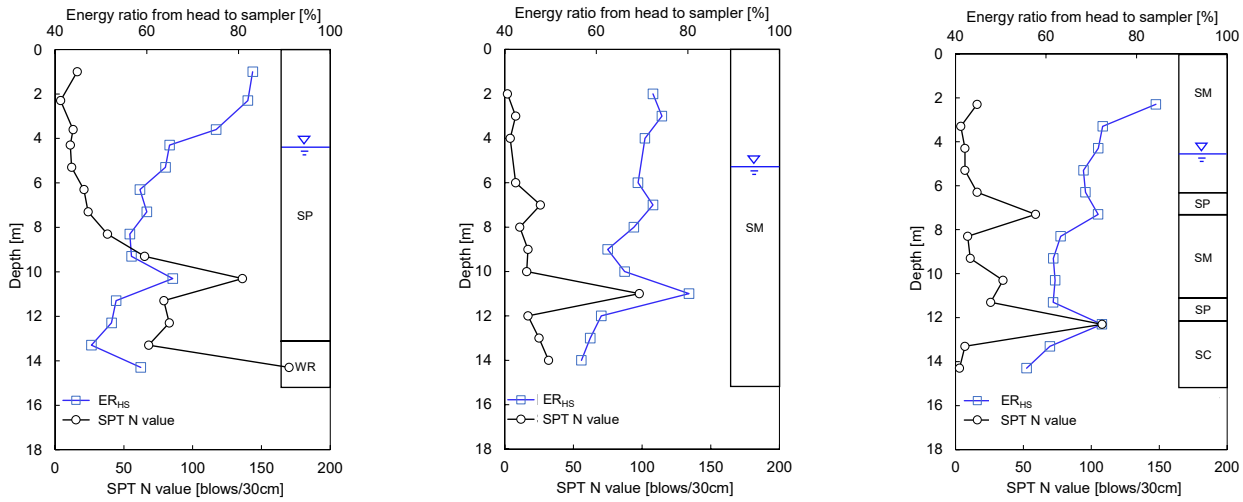

(a) At BH-H (b) At BH-G (c) At BH-P

Fig. 10 SPT N-value (N) and energy ratio from head to sampler (ERHS) according to depth

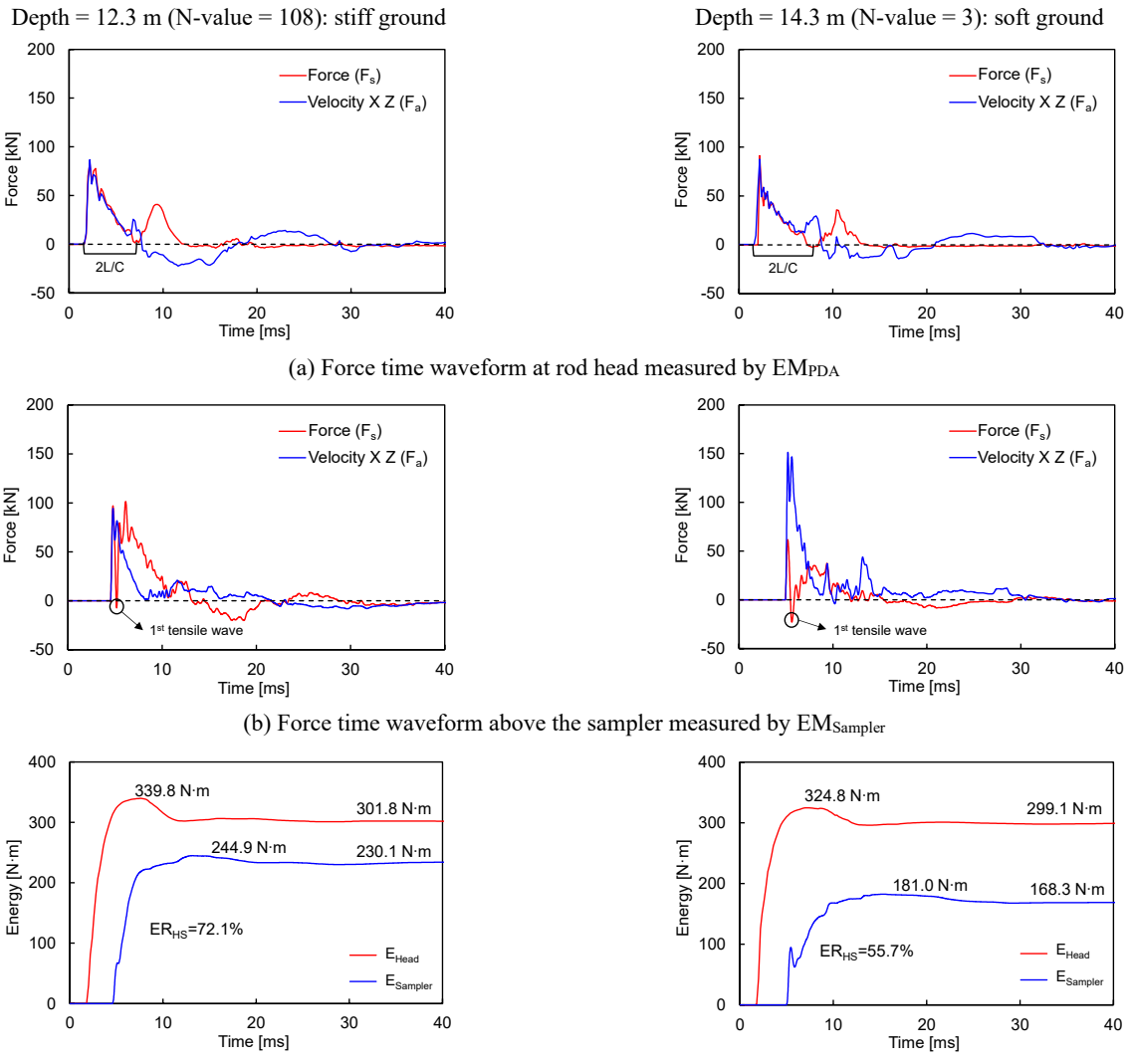

(a) Force time waveform at rod head measured by EM_{PDA}

(b) Force time waveform above the sampler measured by $EM_{Sampler}$

(c) Energy time waveform

Fig. 11 Measured dynamic responses at penetration depths of 12.3, 14.3 m at BH-P

near 2L/C after impact, the particle velocity (V_a) in soft ground (14.3 m depth) is greater than that in stiff ground (12.3 m depth). Force time waveforms measured by $EM_{Sampler}$ are plotted in Fig. 11(b). As the impedance of stiff ground is greater than that of soft ground, the reflection of force waves (F_s) is greater in stiff ground (12.3 m depth) than in soft ground (14.3 m depth). Note that velocity waves (velocity×Z: F_a) are opposite. Furthermore, Fig. 11(b) shows that the peaks of F_s and F_a are similar in stiff ground, but the peak of F_a is larger than that of F_s in soft ground. As the particle velocity becomes double at the free boundary condition (Smith 1960, Skov 1982, Kim *et al*. 2022), the velocity waves (velocity×Z: F_a) are greater than F_s in soft ground.

The energy time waveforms based on the F-V method are calculated using the measured force time waveforms at the rod head and above the SPT sampler at depths of 12.3 m and 14.3 m and are plotted in Fig. 11(c). The peak values of E_{Head} at both depths are 339.8 N·m and 324.8 N·m, and the final values of E_{Head} at both depths are 301.8 N·m and 299.1 N·m, respectively. In other words, E_{Head} decreases by 11.2% in stiff ground (12.3 m depth), and slightly decreases by 7.9% in soft ground (14.3 m depth). Fig. 11(b) shows that in the F_s measured from the $EM_{Sampler}$, a tensile wave occurred immediately after the initial compression wave at both depths. Note that as the $EM_{Sampler}$ is installed directly above the SPT sampler, the arrival time of the initial tensile wave is short (Lukiantchuki *et al*. 2011). The initial tensile wave, which is influenced by the stiffness of the ground, affects reduction of $E_{Sampler}$. As the magnitude of initial tensile wave decreases with an increase in the SPT N-values, the peak value of $E_{Sampler}$ in stiff ground (244.9 N·m) is greater than that in soft ground (181.0 N·m) for similar peak values of E_{Head}. Thus, ER_{HS} in stiff ground at the depth of 12.3 m (72.1%) is greater than that in soft ground at the depth of 14.3 m (55.7%).

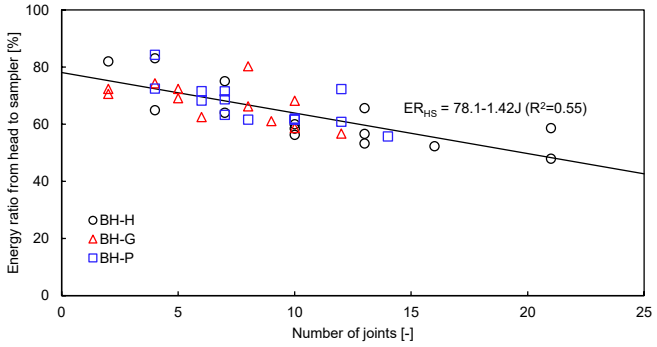

(a) According to the number of joints (J)

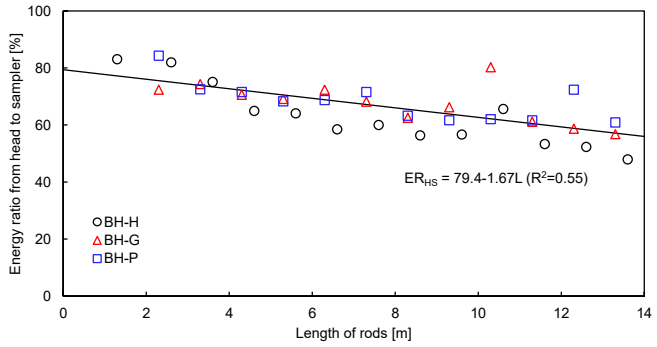

(b) According to the length of driving rods (L)

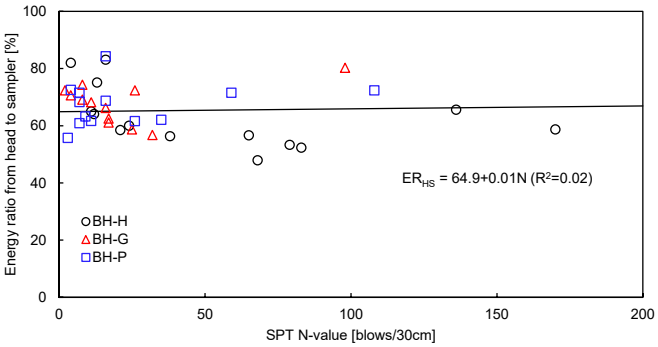

(c) According to the SPT N value (N)

Fig. 12 Energy ratio from head to sampler (ER_{HS})

Table 3 Correlation of ER_{HS} and determination coefficient according to independent variables

Independent variables	Correlation of ER_{HS}	Determination coefficient, R^2	Eq. No.
J	ER_{HS} (%) = 78.1-1.42J	0.55	(11)
L	ER_{HS} (%) = 79.4-1.67L	0.55	(12)
N	ER_{HS} (%) = 64.9+0.01N	0.02	(13)
J, L	ER_{HS} (%) = 79.7-0.77J-0.89L	0.59	(14)
J, N	ER_{HS} (%) = 80.1-2.07J+0.11N	0.69	(15)
L, N	ER_{HS} (%) = 80.1-2.01L+0.06N	0.60	(16)
J, L, N	ER_{HS} (%) = 81.3-1.50J-0.76L+0.11N	0.72	(17)

5.2 Effects of number of joints and length of driving rods

The calculated energy transfer ratio from the rod head to the sampler (ER_{HS}) at three sites were plotted according to the number of joints (J), rod length (L), and SPT N-value (N) in Fig. 12. The ER_{HS} decreases with an increase in the number of joints (J) or in the rod length (L) as shown in Figs. 12(a) and 12(b). However, the ER_{HS} has no significant correlation with N as shown in Fig. 12(c).

Linear regression analyses were conducted to evaluate the correlation among the energy transfer ratio from the rod head to the sampler (ER_{HS}) and the three independent variables (J, L, and N) based on the plotted results. Linear regression analyses can be used to evaluate the correlation between several variables (Seber and Lee 2012, Montgomery *et al.* 2021), and linear polynomials for independent variables were derived to evaluate the correlation. Correlations and determination coefficients between ER_{HS} and independent variables are summarized in Table 3. Table 3 shows that the determination coefficients in correlations between ER_{HS} and J represented by Eq. (11), and between ER_{HS} and L represented by Eq. (12) are 0.55. Note that the correlation between ER_{HS} and N (Eq. (13)) produces the determination coefficient of 0.02, which means that ER_{HS} is unrelated with N. Correlations between the ER_{HS} and two independent variables are described in Eqs. (14)-(16). Eqs. (14)-(16) show that determination coefficients of ER_{HS} with J and L, J and N, and L and N are 0.59, 0.69, and 0.60, respectively. Note that the correlation of ER_{HS} with J and N (Eq. (15)) is better than that of ER_{HS} with L and N (Eq. (16)). Eqs. (15) and (16) suggest that the energy transfer ratio from the rod head to the sampler (ER_{HS}) be more affected by the number of joints (J) than rod length (L) if they are analyzed with the SPT N-value. The correlation of the ER_{HS} with all three independent variables represented in Eq. (17) produces the highest determination coefficient (0.72), which demonstrates that ER_{HS} be related with on soil properties, the number of joints, and the rod length.

As energy loss occurs mainly at the joints due to the impedance difference (Byun and Lee 2013), the ER_{HS} and J should be strongly correlated. Even though the rod length (L) should not affect the energy loss, it is a high correlation with the ER_{HS} because the rod length increases with an increase in the number of joints. Thus, the determination coefficient of the correlation ER_{HS} with J and L is not high

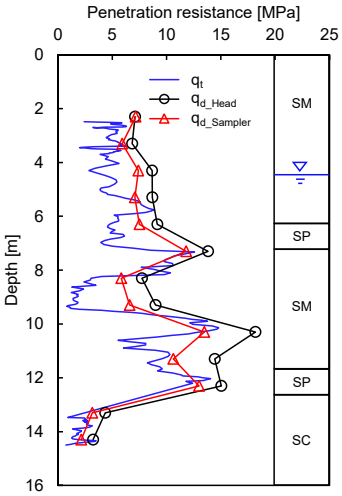

Fig. 13 Corrected cone tip resistance (q_t), and estimated dynamic resistances based on transferred energies into rod head and sampler according to depth (SP, WR, SM and SC denote the poorly graded sand, weathered rock, silty sand, and clayey sand, respectively)

value (0.59) described in Eq. (14). In addition, among the relationships between the ER_{HS} and two variables, the correlation of the ER_{HS} with J and N is highest as J has a greater influence than L. Even though the SPT N-value (N) does not have a direct relationship with the ER_{HS} (Eq. (13)), it improves the correlation of ER_{HS} with other independent variables (J and L) as described in Eqs. (15)-(17). Note that for identical or similar J and L, the ER_{HS} is greatly influenced by the ground condition as plotted in Fig. 10.

5.3 Dynamic resistance vs. static cone tip resistance

For the BH-P site as shown in Fig. 9, the energy-corrected SPT N-value (N_{60}) using the transferred energies into the rod head and the SPT sampler shows a similar trend with the corrected cone tip resistance (q_t). To compare SPT and CPT results, the dynamic resistance (q_d) is calculated using Eq. (10). As the penetration energy ($E_{Penetration}$) can be regarded as E_{Head} or $E_{Sampler}$, two types of dynamic resistances from SPT are obtained using E_{Head} (q_{d_Head}) and $E_{Sampler}$ (q_{d_Samper}). The two types of dynamic resistance and q_t of CPT are plotted in Fig. 13. Fig. 13 shows that the

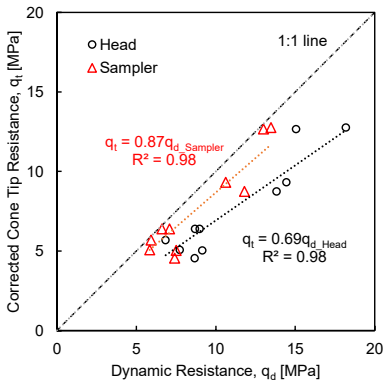

Fig. 14 Corrected cone tip resistance versus dynamic resistances based on transferred energies into rod head and sampler

q_{d_Head} is generally higher than the q_t and $q_{d\_Sampler}$. In addition, the $q_{d\_Sampler}$ is slightly higher than q_t on average.

For the investigation of the relationship between q_d and q_t, q_t is plotted with q_{d_Head} and $q_{d\_Sampler}$ in Fig. 14. Note that as the difference between the q_d and q_t in clay is greater than that in sand due to the damping effect (Gibson and Coyle 1968), the two points obtained in clay ground are excluded in this comparison. The slope of the trend line of q_{d_Head} and q_t and that of $q_{d\_Sampler}$ and q_t are 0.69 and 0.87, respectively. The determination coefficients of both trend lines are 0.98. When q_d is calculated by considering $E_{Penetration}$ as E_{Head}, the energy losses due to the number of joints, rod length, and friction between the SPT sampler and soils are not accurately counted (Odebrecht *et al.* 2004). Thus, the dynamic resistance using E_{Head} (q_{d_Head}) may be overestimated. On the other hand, $q_{d\_Sampler}$ is not considered in the energy loss of the friction between the SPT sampler and soils, but the energy losses of J and L are considered. Therefore, the dynamic resistance using $E_{Sampler}$ ($q_{d\_Sampler}$) is slightly overestimated compared to q_t.

According to the relationship between $q_{d\_Sampler}$ and q_t, the friction between the SPT sampler and soils is estimated to be approximately 13% of $q_{d\_Sampler}$ on average in these field tests (Fig. 14). Note that the friction between the SPT sampler and soils depends on the soil type and sampler geometry. Despite this limitation, as the transferred energy into the sampler ($E_{Sampler}$) is comparable to the actual penetration energy, and the $q_{d\_Sampler}$ is comparable to the q_t. Thus, $q_{d\_Sampler}$ may be more effectively used for the estimation of the dynamic resistance and for the correlation with the corrected cone tip resistance.

6. Conclusions

In this study, the transferred energies into the rod head (E_{Head}) and into the SPT sampler ($E_{Sampler}$) were measured to evaluate the effects of the number of joints and rod length on the energy transfer ratio. The energy modules configured with the accelerometer and load cell were used to measure the transferred energies into the rod head and into the SPT sampler. Furthermore, the commercial energy module was used to measure the transferred energy into the rod head. The SPTs were conducted at Hanam, Gongju, and Pohang sites in Korea. For the Pohang site, CPT was conducted near the SPT borehole. According to the depth, the acceleration and force signals were obtained using the energy modules during SPTs, and the transferred energies (E_{Head} and $E_{Sampler}$) were subsequently calculated based on the force-velocity (F-V) method. The energy ratio from the head to the sampler (ER_{HS}), which is the ratio of the transferred energy into the SPT sampler to that into the head, was correlated with the number of joints (J), rod length (L), and SPT N-value (N). In addition, the dynamic resistances from the SPT, which were calculated by using both E_{Head} and $E_{Sampler}$, were compared with the corrected cone tip resistance (q_t) from CPT. The main observations of this study are as follows:

- Energy transfer ratio into the head (ETR_{Head}) at the three sites are generally constant along the depth, and energy transfer ratios into the sampler ($ETR_{Sampler}$) generally decrease with the depth. Thus, the energy ratio from the head to the sampler (ER_{HS}) gradually decreases with an increase in the depth in all sites. The higher values of ER_{HS}, however, are obtained at stiff ground, in which the SPT N-values are more than 100 blows/30 cm, because the magnitude of the initial tensile wave in stiff ground is smaller than that in soft ground.
- The energy ratio from head to the sampler (ER_{HS}) gradually decreases with an increase in the number of joints (J) or in the rod length (L), but it has no significant correlation with SPT N-value (N). However, in the correlation of the ER_{HS} with two variables (J and N, or L and N), N improves the correlation of ER_{HS} with other independent variables (J or L). As the correlation of the ER_{HS} with all three independent variables (J, L, and N) is highest, the ER_{HS} may be effectively estimated using the number of joints (J), the rod length (L), and SPT N-value (N).
- The dynamic resistance based on E_{Head} (q_{d_Head}) is greater than the corrected cone tip resistance (q_t), as the energy losses due to the number of joints, rod length and friction occurred at the SPT sampler are not accurately counted. As the $E_{Sampler}$ considers the energy losses from J and L, except the friction occurred at the SPT sampler, the dynamic resistance using $E_{Sampler}$ ($q_{d\_Sampler}$) is slightly greater than q_t. Thus, $q_{d\_Sampler}$ may be effectively used for the estimation of the dynamic resistance.

Acknowledgments

This work is supported by Smart City R&D project of the Korea Agency for Infrastructure Tech-nology Advancement (KAIA) grant funded by the Ministry of Land, Infrastructure and Transport (Grant 22NSPSB149830-05).

References

ASTM D422 (2007), Standard Test Method for Particle-size Analysis of Soils, ASTM International, West Conshohocken, PA, USA.

ASTM D4253 (2006), Standard Test Methods for Maximum Index Density and Unit Weight of Soils Using a Vibratory Table, ASTM International, West Conshohocken, PA, USA.

ASTM D4254 (2006), Standard Test Methods for Minimum Index Density and Unit Weight of Soils and Calculation of Relative Density, ASTM International, West Conshohocken, PA, USA.

ASTM D4318 (2005), Standard Test Methods for Liquid Limit, Plastic Limit, and Plasticity Index of Soils, ASTM International, West Conshohocken, PA, USA.

ASTM D4633 (2010), Standard Test Method for Energy Measurement for Dynamic Penetrometers, ASTM International, West Conshohocken, PA, USA.

ASTM D854 (2009), Standard Test Methods for Specific Gravity of Soil Solids by Water Pycnometer, ASTM International, West Conshohocken, PA, USA.

Bahari, B., Hwang, W., Kim, T. H. and Song, Y.S. (2020), "Estimation of liquefaction potential in Eco-Delta City (Busan) using different approaches with effect of fines content", *Int. J. Geo-Eng.*, **11**(1), 1-30. https://doi.org/10.1186/s40703-020-00121-4

Bowles, L.E. (1996), *Foundation Analysis and Design*, McGraw-Hill, New York, NY, USA.

Butler, J.J., Caliendo, J.A. and Goble, G.G. (1998), "Comparison of SPT energy measurement methods", In: *Geotechnical Site Characterization*, pp. 901-905.

Byun, Y.H. and Lee, J.S. (2013), "Instrumented dynamic cone penetrometer corrected with transferred energy into a cone tip: a laboratory study", *Geotech. Test. J.*, **36**(4), 533-542. https://doi.org/10.1520/GTJ20120115

Byun, Y.H., Kim, J.H. and Lee, J.S. (2013), "Cone penetrometer with a helical-type outer screw rod for evaluation of the subgrade condition", *J. Transport. Eng.*, **139**(2), 115-122. https://doi.org/10.1061/(ASCE)TE.1943-5436.0000504

Byun, Y.H., Yoon, H.K., Kim, Y.S., Hong, S.S. and Lee, J.S. (2014), "Active layer characterization by instrumented dynamic cone penetrometer in Ny-Alesund, Svalbard", *Cold Regions Sci. Technol.*, **104**, 45-53. https://doi.org/10.1016/j.coldregions.2014.04.003

Byun, Y.H., Hong, W.T. and Lee, J.S. (2015), "Characterization of railway substructure using a hybrid cone penetrometer", *Smart Struct. Syst., Int. J.*, **15**(4), 1085-1101. http://dx.doi.org/10.12989/sss.2015.15.4.1085

Clayton, C.R. (1995), "The standard penetration test (SPT): methods and use", Construction Industry Research and Information Association, Construction Industry Research and Information Association, London, UK.

Cubrinovski, M. and Ishihara, K. (1999), "Empirical correlation between SPT N-value and relative density for sandy soils", *Soils Found.*, **39**(5), 61-71. https://doi.org/10.3208/sandf.39.5_61

Das, B.M., Sivakugan, N. and Atalar, C. (2012), "Maximum and minimum void ratios and median grain size of granular soils: their importance and correlations with material properties", *Proceedings of the 3rd International Conference on New Developments in Soil Mechanics and Geotechnical Engineering*, Near East University, Nicosia, North Cyprus, June.

Decourt, L., Muromachi, T., Nixon, I.K., Schmertmann, J.H. and Thorburn, S. (1988), "Standard penetration test (SPT): International reference test procedure", In: *International Symposium on Penetration Testing*, ISOPT-1, Balkema, São Paulo, Brazil, March.

Ghali, M., Chekired, M. and Karray, M. (2020), "Framework to improve the correlation of SPT-N and geotechnical parameters in sand", *Acta Geotechnica*, **15**(3), 735-759. https://doi.org/10.1007/s11440-018-0745-3

Gibson, G.C. and Coyle, H.M. (1968), "Soil damping constants related to common soil properties in sands and clays", Texas Transportation Institute, Texas A&M University, College Station, TX, USA.

Hatanaka, M. and Uchida, A. (1996), "Empirical correlation between penetration resistance and internal friction angle of sandy soils", *Soils Found.*, **36**(4), 1-9. https://doi.org/10.3208/sandf.36.4_1

Hettiarachchi, H. and Brown, T. (2009), "Use of SPT blow counts to estimate shear strength properties of soils: energy balance approach", *J. Geotech. Geoenviron. Eng.*, **135**(6), 830-834. https://doi.org/10.1061/(ASCE)GT.1943-5606.0000016

Hong, W.T., Byun, Y.H., Kim, S.Y. and Lee, J.S. (2016), "Cone penetrometer incorporated with dynamic cone penetration method for investigation of track substructures", *Smart Struct. Syst., Int. J.*, **18**(2), 197-216. https://doi.org/10.12989/sss.2016.18.2.197

Hong, W.T., Kim, S.Y. and Lee, J.S. (2022), "Evaluation of driving energy transferred to split spoon sampler for accuracy improvement of standard penetration test", *Measurement*, **188**, 110384. https://doi.org/10.1016/j.measurement.2021.110384

Kianirad, E., Gamache, R.W., Brady, D. and Alshawabkeh, A.N. (2011), "Equivalent quasi-static estimation of dynamic penetration force for near surface soil characterization", In: *Geo-Frontiers 2011: Advances in Geotechnical Engineering*, ASCE, Reston, VA, USA.

Kim, S.Y., Hong, W.T. and Lee, J.S. (2019), "Role of the coefficient of uniformity on the California bearing ratio, penetration resistance, and small strain stiffness of coarse arctic soils", *Cold Regions Sci. Technol.*, **160**, 230-241. https://doi.org/10.1016/j.coldregions.2019.02.012

Kim, S.Y., Lee, J.S., Tutumluer, E. and Byun, Y.H. (2022), "Dynamic response of free-end rod with consideration of wave frequency.", *Geomech. Eng., Int. J.*, **28**(1), 25-33. https://doi.org/10.12989/gae.2022.28.1.025

Kovacs, W.D. (1979), "Velocity measurement of free-fall SPT hammer", *J. Geotech. Geoenviron. Eng.*, **105**(1), 1-10. https://doi.org/10.1061/AJGEB6.0000748

Kovacs, W.D. and Salomone, L.A. (1982), "SPT hammer energy measurement", *J. Geotech. Geoenviron. Eng.*, **108**(4), 599-620. https://doi.org/10.1061/AJGEB6.0001278

Kulhawy, F.H. and Mayne, P.W. (1990), "Manual on estimating soil properties for foundation design", Geotechnical Engineering Group, Cornell University, Ithaca, NY, USA.

Lee, J.S. and Byun, Y.H. (2020), "Instrumented Cone Penetrometer for Dense Layer Characterization", *Sensors*, **20**(20), 1-19. https://doi.org/10.3390/s20205782

Lee, W.J., Yu, J.M., Cho, S.M. and Ryu, D.H. (2001), "Effect of rod length on the evaluation of SPT rod energy ratio", *Korean Geoenviron. Soc.*, **9**, 193-198. [In Korean] https://doi.org/10.1061/(ASCE)GT.1943-5606.0000236

Lee, C., Lee, J.S., An, S. and Lee, W. (2010), "Effect of secondary impacts on SPT rod energy and sampler penetration", *J. Geotech. Geoenviron. Eng.*, **136**(3), 522-526. https://doi.org/10.1061/(ASCE)GT.1943-5606.0000236

Lukiantchuki, J.A., Esquivel, E.R. and Bernardes, G.P. (2011), "Interpretation of force and acceleration signals during hammer impact in SPT tests", *Proceedings of 14th Pan-American Conference on Soil Mechanics and Geotechnical Engineering*, Toronto, Canada.

Lee, J.S., Kim, S.Y., Hong, W.T. and Byun, Y.H. (2019), "Assessing subgrade strength using an instrumented dynamic cone penetrometer", *Soils Found.*, **59**(4), 930-941. https://doi.org/10.1016/j.sandf.2019.03.005

Marcuson, W.F. and Bieganousky, W.A. (1977), "SPT and relative

density in coarse sands", *J. Geotech. Eng. Div.*, **103**(11), 1295-1309. https://doi.org/10.1061/AJGEB6.0000521

Melzer, K.J. (1971), "Standard penetration test and relative density", M-71-1; Army Engineering Waterways Experiment Station.

Montgomery, D.C., Peck, E.A. and Vining, G.G. (2021), *Introduction to linear regression analysis*, John Wiley & Sons, New York, NY, USA.

Mujtaba, H., Farooq, K., Sivakugan, N. and Das, B.M. (2018), "Evaluation of relative density and friction angle based on SPT-N values", *KSCE J. Civil Eng.*, **22**(2), 572-581. https://doi.org/10.1007/s12205-017-1899-5

Odebrecht, E., Schnaid, F., Rocha, M.M. and Bernardes, G.P. (2004), "Energy measurements for standard penetration tests and the effects of the length of rods", *Geotech. Geophys. Site Characteriz.*, **1**, 351-358.

Robertson, P.K. and Wride, C.E. (1997), "Cyclic liquefaction and its evaluation based on SPT and CPT: Seismic Short Course on Evaluation and Mitigation of Earthquake Induced Liquefaction Hazards", In: *NCEER Workshop*, San Francisco, CA, USA.

Schmertmann, J.H. and Palacios, A. (1979), "Energy dynamics of SPT", *J. Geotech. Eng. Div.*, **105**(8), 909-926. https://doi.org/10.1061/AJGEB6.0000839

Schnaid, F., Odebrecht, E., Rocha, M.M. and de Paula Bernardes, G. (2009), "Prediction of soil properties from the concepts of energy transfer in dynamic penetration tests", *J. Geotech. Geoenviron. Eng.*, **135**(8), 1092-1100. https://doi.org/10.1061/(ASCE)GT.1943-5606.0000059

Schnaid, F., Lourenço, D. and Odebrecht, E. (2017), "Interpretation of static and dynamic penetration tests in coarse-grained soils", *Géotechnique Lett.*, **7**(2), 113-118. https://doi.org/10.1680/jgele.16.00170

Seber, G.A. and Lee, A.J. (2012), *Linear regression analysis*, John Wiley & Sons, New York, NY, USA.

Seed, B.H., Tokimatsu, K., Harder, L.F. and Chung, R.M. (1985), "Influence of SPT procedures in soil liquefaction resistance evaluations", *J. Geotech. Eng.*, **111**(12), 1425-1445. https://doi.org/10.1061/(ASCE)0733-9410(1985)111:12(1425)

Seo, M.J., Han, K., Park, J.B., Jeong, K.H. and Lee, J.S. (2021), "End bearing capacity of embedded pile with inclined base plate: Field dynamic and static tests", *Geomech. Eng., Int. J.*, **26**(3), 261-274. https://doi.org/10.12989/gae.2021.26.3.261

Sjoblom, D., Bischoff, J. and Cox, K. (2002), "SPT energy measurements with the PDA", *Proceedings of the 2nd International Conference on the Application of Geophysicals and NDT Methodologies to Transportation Facilities and Infrastructure*, Los Angeles, CA, USA, April.

Skempton, A.W. (1986), "Standard penetration test procedures and the effects in sands of overburden pressure, relative density, particle size, ageing and overconsolidation", *Geotechnique*, **36**(3), 425-447. https://doi.org/10.1680/geot.1986.36.3.425

Skov, R. (1982), "Evaluation of stress wave measurements", DMT, Grümdungstechnik, Hamburg, Germany.

Smith, E.A. (1960), "Pile-driving analysis by the wave equation", *Am. Soc. Civil Engr. Transact.*, **86**, 35-61. https://doi.org/10.1061/JSFEAQ.0000281

Yoon, H.K. and Lee, J.S. (2012), "Microcones configured with full-bridge circuits", *Soil Dyn. Earthq. Eng.*, **41**, 119-127. https://doi.org/10.1016/j.soildyn.2012.05.013